

1 **A Consolidated Database of Mercury Observations for Permafrost Regions**

2 [Christine L. Olson](#)¹, [Kevin Schaefer](#)¹, [Alyssa Azaroff](#)², [Hélène Angot](#)³, [Sasiri Bandara](#)⁴, [Thomas](#)
3 [A. Douglas](#)⁵, [Bo Elberling](#)⁶, [Maria Florencia Fahnestock](#)⁷, [Xinbin Feng](#)⁸, [Charlotte Haugk](#)²,
4 [Gustaf Hugelius](#)², [Erfan Jahangir](#)³, [Sofi Jonsson](#)², [Shichang Kang](#)^{9,10}, [Adam Kirkwood](#)¹¹,
5 [Jennifer Korosi](#)¹², [Igor Lehnerr](#)¹³, [Artem Lim](#)¹⁴, [Rinat Manasyrov](#)¹⁴, [Dmitriy Moskovchenko](#)¹⁵,
6 [Mina Nasr](#)¹⁶, [Daniel Obrist](#)¹⁸, [David Olefeldt](#)¹⁷, [Connor Olson](#)^{1,19}, [Oleg Pokrovsky](#)²⁰, [Laura](#)
7 [Sereni](#)³, [Sarah Shakil](#)²¹, [M. Isabel Smith](#)²², [Jens Søndergaard](#)²³, [Jeroen Sonke](#)²⁰, [Kasia](#)
8 [Staniszewska](#)⁴, [Jens Strauss](#)²⁴, [Kyra St. Pierre](#)²⁵, [Lauren Thompson](#)¹⁷, [Andrey Yurtaev](#)¹⁴, [Yanxu](#)
9 [Zhang](#)²⁶, and [Scott Zolkos](#)²⁷.

- 10 ¹ [University of Colorado, Boulder, USA](#)
- 11 ² [Stockholm University, Sweden](#)
- 12 ³ [Univ. Grenoble Alpes, CNRS, INRAE, IRD, Grenoble INP, IGE, France](#)
- 13 ⁴ [University of Alberta, Edmonton, Alberta, Canada](#)
- 14 ⁵ [U.S. Army Cold Regions Research and Engineering Laboratory Fort Wainwright, USA](#)
- 15 ⁶ [University of Copenhagen, Denmark](#)
- 16 ⁷ [University of New Hampshire, USA](#)
- 17 ⁸ [Institute of Geochemistry, Chinese Academy of Sciences, China](#)
- 18 ⁹ [Institute of Mountain Hazards and Environment, Chinese Academy of Sciences](#)
- 19 ¹⁰ [University of Chinese Academy of Sciences, China](#)
- 20 ¹¹ [Carleton University, Canada](#)
- 21 ¹² [York University, Canada](#)
- 22 ¹³ [Department of Geography, Geomatics and Environment, University of Toronto Mississauga, Canada](#)
- 23 ¹⁴ [Tomsk State University, Russia](#)
- 24 ¹⁵ [Tyumen Scientific Centre SB RAS, Russia](#)
- 25 ¹⁶ [Environment and Protected Areas, Government of Alberta, Canada](#)
- 26 ¹⁷ [University of California Agricultural and Natural Resources, USA](#)
- 27 ¹⁸ [Department of Renewable Resources, University of Alberta, Edmonton, Alberta, Canada](#)
- 28 ¹⁹ [Harvard University, USA](#)
- 29 ²⁰ [Géosciences Environnement Toulouse, CNRS/IRD/Université de Toulouse, 31400 France](#)
- 30 ²¹ [Department of Ecology and Genetics; Limnology, Uppsala University, Uppsala, Sweden](#)
- 31 ²² [University of Southern California, USA](#)
- 32 ²³ [Aarhus University, Denmark](#)
- 33 ²⁴ [Alfred Wegener Institute Helmholtz Centre for Polar and Marine Research, Germany](#)
- 34 ²⁵ [University of Ottawa, Canada](#)
- 35 ²⁶ [Tulane University, USA](#)
- 36 ²⁷ [Woodwell Climate Research Center, USA](#)

37
38 **E-mail:** christine.olson@colorado.edu, kevin.schaefer@colorado.edu

39 **Keywords:** mercury (Hg), PermHg database, permafrost, soil, water, vegetation, lake sediment

40 **Abstract**

41 ~~S~~Permafrost soils across permafrost regions are one of the largest terrestrial pools of mercury
42 (Hg) in the world, storing an estimated 500–1500 Gg of Hg in the top three meters of soil.
43 Ongoing climate-driven thaw threatens to release this legacy Hg into the environment. Efforts to
44 quantify and model this pool have been hindered by a lack of harmonized, spatially resolved

Formatted: Font: (Default) Times New Roman

Formatted: Font: 10 pt, Font color: Auto, Superscript

Formatted: Font: 10 pt, Font color: Auto

Formatted: No Spacing

Formatted: Font: 10 pt, Font color: Auto, Superscript

Formatted: Font: 10 pt, Font color: Auto, Superscript

Formatted: Font: 10 pt, Font color: Auto, Superscript

Formatted: Font: 10 pt, Font color: Auto, Superscript

Formatted: Font: 10 pt, Font color: Auto, Superscript

Formatted: Font: 10 pt, Font color: Auto, Superscript

Formatted: Font: 10 pt, Font color: Auto, Superscript

Formatted: Font: 10 pt, Font color: Auto, Superscript

Formatted: Font: 10 pt, Font color: Auto

Formatted: No Spacing

Formatted: Font: 10 pt, Font color: Auto, Superscript

Formatted: Font: 10 pt, Font color: Auto, Superscript

Formatted: Font: 10 pt, Font color: Auto, Superscript

Formatted: Font: 10 pt, Font color: Auto, Superscript

Formatted: Font: 10 pt, Font color: Auto, Superscript

Formatted: Font: 10 pt, Font color: Auto, Superscript

Formatted: Font: 10 pt, Font color: Auto, Superscript

Formatted: Font: 10 pt, Font color: Auto, Superscript

Formatted: Font: 10 pt, Font color: Auto, Superscript

Formatted: Font: 10 pt

Formatted: Font: 10 pt, Font color: Auto, Superscript

Formatted: Font: 10 pt, Font color: Auto, Superscript

Formatted: Font: 10 pt, Font color: Auto, Superscript

Formatted: Font: 10 pt, Font color: Auto, Superscript

Formatted: Font: 10 pt, Font color: Auto, Superscript

Formatted: Font: 10 pt, Font color: Auto, Superscript

Formatted: Font: 10 pt, Font color: Auto, Superscript

Formatted: Font: (Default) +Body (Aptos), Font color: Auto

Formatted: No Spacing

45 observations. To address this, we compiled a database of 117,802 Hg observations collected
46 between 1988 and 2022 from 59 studies across Arctic, sub-Arctic, and alpine permafrost regions
47 of the Northern Hemisphere, including North America, northern Europe, Eurasia, and the
48 Tibetan Plateau. The database includes Hg concentration measurements in solid materials—such
49 as soil, leaves, roots, and wood, and litter—as well as in water samples from soil porewater,
50 lakes, and rivers across the northern hemisphere permafrost domain. The database enables cross-
51 site synthesis, model calibration and evaluation, and environmental assessments by standardizing
52 and harmonizing data from diverse sources. Data harmonization steps standardization included
53 unit conversion, categorization of observations by type, and quality-control measures-procedures
54 to ensure consistency across studies. Analytical uncertainty was preserved where reported in
55 source studies, and qualitative quality control uncertainty indicators – including range and
56 outlier flags – were applied where uncertainty information was incomplete or
57 heterogeneous to support data screening and interpretation. Mercury concentrations vary widely
58 across observations, with lake sediment showing the highest median values (70 ng g⁻¹, IQR: 45-
59 116), followed by soil (50 ng g⁻¹, IQR: 32-90), and vegetation (15 ng g⁻¹, IQR: 9-33). Water
60 observations (total Hg) had a median of 2 ng L⁻¹ (IQR: 2-6). Statistically significant differences
61 in Hg concentrations among observation types were observed at both global and regional scales,
62 consistently generally following the pattern: lake sediment > soil > vegetation, although this
63 ordering is sensitive to regional sampling distribution → water. These patterns, along with spatial
64 and observation-type biases, highlight the need for improved coverage in underrepresented
65 regions such as Eurasia. The database is freely accessible through Zenodo under the concept DOI
66 10.5281/zenodo.18300989 (all versions), to support ongoing research and model development in
67 Arctic and sub-Arctic Hg cycle studies.

68 1. Introduction

69 Permafrost-region soils ~~Permafrost soils also~~ contain the largest terrestrial pool of Hg in the
70 world (Schuster et al., 2018; Olson et al., 2018; Lim et al., 2020). Anthropogenic activities and
71 natural sources such as volcanoes and rock weathering release Hg into the environment
72 (Fitzgerald and Lamborg, 2014). Mercury in permafrost primarily originates from long-range
73 atmospheric transport of Hg from lower latitudes (Dastoor et al., 2022). About two-thirds of Hg
74 in remote permafrost regions is deposited to terrestrial ecosystems where it accumulates in soils
75 via vegetation uptake and transfer through litterfall and throughfall (Obrist et al., 2017; Olson et

76 al., 2018, 2019). As permafrost thaws, Hg bound to organic rich matter may become mobilized
77 into terrestrial and aquatic ecosystems (Chételat et al., 2022; Jonsson et al., 2022; St. Pierre et al.,
78 2018). In addition to thaw-driven mobilization, rapid Arctic landscape change, including
79 thermokarst development, erosion, and shifting sediment transport pathways, may further alter
80 Hg redistribution and export across northern river and coastal systems (Tiang et al., 2026). Once
81 mobilized, it can be transported to wetlands, rivers (Fabre et al., 2024; Zolkos et al., 2020), lakes
82 (MacMillan et al., 2015; Varty et al., 2021), and coastal (Giest et al., 2025) environments where
83 microbial processes can convert it to methylmercury (MeHg) – a highly toxic and
84 bioaccumulative form (Jonsson et al., 2022). As climate warming accelerates, this sequence of
85 thaw-driven mobilization, transport, and methylation could trigger a permafrost–Hg feedback
86 with far-reaching implications for ecosystem and human health, particularly for Arctic and sub-
87 Arctic communities reliant on aquatic foods seafood as a dietary staple (Schaefer et al., 2020;
88 Basu et al., 2022; Gartler et al., 2025). Understanding the complete terrestrial Hg budget—
89 including vegetation-mediated inputs—is critical for projecting how climate change will alter
90 global Hg cycling.

91 Permafrost regions play a critical role in regulating both local and global Hg cycling. Despite
92 its importance, observational data from these regions remain spatially limited and are rarely
93 synthesized across media (e.g., soil, vegetation, water sediments). As a result, many global Hg
94 budgets either exclude these areas or rely on highly uncertain estimates (Outridge et al., 2018;
95 Sonke et al., 2023; Zhang et al., 2023). Although measurements exist, they are dispersed in the
96 literature and have not been integrated into forms usable for larger-scale modeling or policy
97 assessments. Current global budgets incorporate detailed estimates of anthropogenic and natural
98 emissions, wet and dry deposition fluxes, and reservoirs in the ocean, land, and vegetation, yet
99 cold-region biogeochemistry and permafrost processes are inadequately represented. An
100 improved understanding of the global Hg cycle—especially in permafrost—is critical to our
101 understanding of the global Hg cycle and to effectively monitor reduction efforts under
102 international frameworks such as the Minamata Convention on Mercury. An integrated database
103 of available Hg observations in permafrost regions is needed to better represent this outsized
104 global pool.

105 Mercury measurements in permafrost regions remain spatially limited, fragmented across
106 observation types, and largely unintegrated across studies (Arctic Monitoring and Assessment
107 Programme, 2022). Permafrost soil inventories vary widely – from 500-1500 Gg of Hg in the top
108 three meters of soil—due to sparse and spatially unevenly distributed measurements (Schuster et
109 al., 2018; Olson et al., 2018; Lim et al., 2020). Large-scale extrapolations like these rely on the
110 upscaling of localized data using carbon content and Hg-to-carbon ratios from a few accessible
111 regions, leading to geographic biases in global estimates (Lim et al. 2020). In addition,
112 insufficient stratification of observations by ecosystem or soil type (e.g., organic vs. mineral
113 soils) limits the accuracy of Hg storage estimates and the ability to capture spatial heterogeneity.
114 Expanding observational coverage across permafrost regions and ensuring representation across
115 key soil types in permafrost regions are essential to constrain these estimates and reduce
116 uncertainty. Vegetation measurements are even more rare and not co-located with soil Hg
117 measurements, despite vegetation being a key pathway for Hg deposition and transfer to soils
118 through litterfall and wood decomposition. This process plays a crucial role in the accumulation
119 of Hg in permafrost over time, as plant-derived organic matter—and its associated Hg—is buried
120 and frozen. Without co-located vegetation and soil measurements, it is difficult to reconstruct
121 historical Hg inputs and constrain the drivers of current permafrost Hg inventories. Aquatic
122 systems are another critical component, acting as downstream receptors of Hg mobilized from
123 thawing permafrost. In these environments, certain conditions promote the microbial conversion
124 of inorganic Hg to MeHg—a potent neurotoxin that bioaccumulates in food webs and poses the
125 greatest risk to wildlife and human health. Distinct methylation hotspots have been identified in
126 wetlands (Thompson et al., 2023), ponds (MacMillan et al., 2015), and lakes (Jonsson et al.,
127 2022); however, limited data on Hg inputs and outputs hinders our ability to quantify fluxes and
128 establish clear linkages with surrounding terrestrial sources. In permafrost regions, rivers such as
129 the Yukon, Mackenzie, and Ob show high seasonal variability in Hg fluxes, peaking during
130 spring thaw and snowmelt (Sonke et al., 2018; Zolkos et al., 2020). Exports of Hg from streams
131 and rivers in permafrost are sparse and vary widely, driven by differences in land cover, geology,
132 and watershed complexity. This lack of integrated data across observation types hinders our
133 ability to predict future ecological impacts and to quantify the growing contribution of thawing
134 permafrost Hg to the global budget. Consolidating existing observations is therefore a critical

135 first step towards improving predictive models, monitoring strategies, and broader scientific
136 analyses (Horsburgh et al., 2009).

137 This paper introduces the PermHg database, developed through an extensive effort to
138 compile, standardize, and harmonize Hg observations from permafrost-affected environments.
139 The database includes both published and unpublished data on Hg concentrations in soil, aquatic
140 systems, and vegetation across permafrost regions. The goal is to support synthesis efforts,
141 model development, and risk assessment. By improving access to Hg observations in cold-
142 region systems, the PermHg database provides a robust, centralized platform that can be used to
143 enhance our understanding of permafrost landscapes and to help identify implications for
144 northern high-latitude ecosystems.

146 2. Methods

147 We compiled Hg observations by surveying peer-reviewed literature via Web of Science and
148 other scholarly databases, supplemental materials, and open-access data repositories, as well as
149 incorporating unpublished measurements contributed directly by collaborating researchers. The
150 PermHg database is the result of numerous research groups from around the world combining
151 original measurements collected in permafrost regions. We sought to prioritize primary
152 observations, although some observations are from prior synthesis papers. All observations are
153 linked to their original source through a paper identifier and are documented in a comprehensive
154 data source inventory provided with the database. During compilation, records were screened for
155 duplication using site information, coordinates, and reported values; no duplicate records were
156 identified. Data inclusion required sufficient metadata (e.g., location and units), and records
157 lacking essential information were excluded during initial data extraction. All nomenclature,
158 units, and formats were standardized into a single harmonized database for general use. While
159 the database is comprehensive, its completeness is limited by geographic bias in the published
160 record, variable reporting standards, and uneven coverage across ecosystem types. Descriptions
161 of observation types, standardization procedures, and methodologies are detailed below. This
162 will be one of the first open sources, integrated global permafrost Hg databases combining soil,
163 sediment, aquatic systems, and vegetation observations on a large scale.

Formatted: Font: (Default) Times New Roman

Formatted: Normal, Indent: First line: 0.25", Line spacing: 1.5 lines

164 In addition to primary literature sources, a subset of soil permafrost mercury observations
165 was sourced from an independently curated database developed by the Bolin Centre for Climate
166 Research (<https://doi.org/10.17043/azaroff-2026-permafrost-mercury-1>). These data are archived
167 separately and contribute harmonized permafrost mercury observations and associated metadata
168 that complement the broader PermHg compilation.

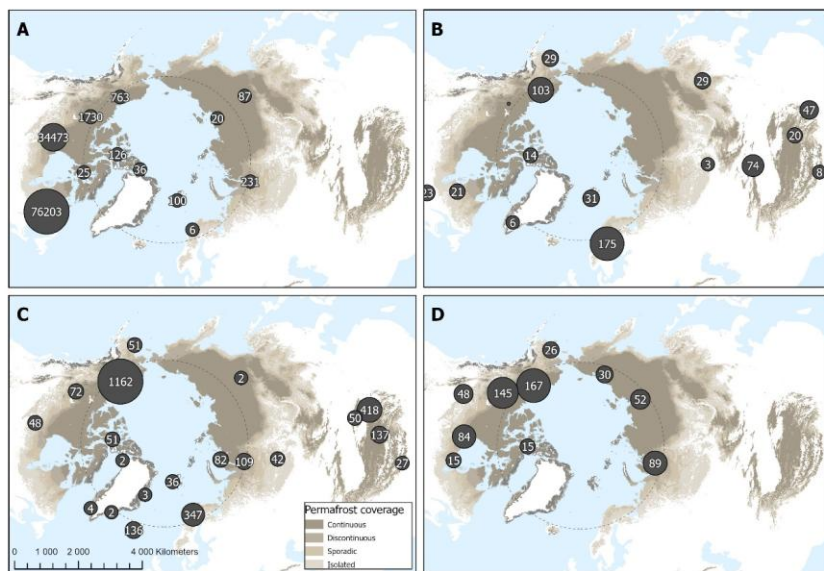
Formatted: Font: Not Bold, Highlight

169 2.1. Study Area

170 The database includes observations from Arctic, sub-Arctic, and alpine permafrost
171 regions in the Northern Hemisphere, including the Tibetan Plateau. Site selection was based on
172 geographic and climatic criteria guided by the modeled permafrost extent and ground
173 temperature map of Obu et al. (2019a). Specifically, we included areas with a modeled
174 probability of permafrost occurrenceprobability of $\geq 10\%$ or greater and mean annual ground
175 temperature below 0°C , capturing a range of permafrost zones from continuous to isolated (Obu
176 et al., 2019a). Lower probability isolated permafrost patches (<10%) shown in Figure 1 were
177 included only as part of the background permafrost map visualization and were not used during
178 database screening.

179 Vegetation cover types for plant Hg data were classified using the circumpolar vegetation
180 map from the ABCflux database (Virkkala et al., 2022). These include land cover classes such as
181 mixed and needleleaf forests, boreal and tundra wetlands, and shrub and barren tundra.
182 Observation locations were overlain on the land cover map to assign the dominant vegetation
183 type for each observation. This enables grouping of observations by ecosystem, which may aid in
184 identifying Hg uptake patterns across different environmental conditions. Note that spatial
185 resolution of the land cover database may be limited in some areas; however, using a
186 standardized land cover supports future ecological comparisons and model parameterization
187 efforts.

188 A map of the geographic domain is provided in **Fig. 1** to visualize the spatial distribution
189 of data points and overall coverage of the study. The figure includes a map of Hg observations,
190 with spatial coverage differentiated by observation type. Circle size and embedded numbers
191 indicate observation density, while circle color indicates observation type (e.g., soil, water,
192 vegetation, or lake sediment). The background shading represents the likelihood of permafrost
193 occurrence, based on the probabilistic map from Obu et al. (2019b).



194
 195 **Figure 1.** The map shows the global PermHg observation locations for (a), lake sediment, (b) vegetation
 196 (c) soil and (d) water. Water data includes observations in lakes, rivers, creeks, oceans, wetlands, ponds,
 197 and soil porewater. Circle size and numbers show observation density or counts per area. The
 198 background shading shows the modeled probability of different types of permafrost occurrence based on
 199 criteria defined in Obu et al., 2019. Permafrost is classified by probability: continuous (>0.9),
 200 discontinuous (0.5–0.9), sporadic (0.1–0.5), and isolated patches (0.001–0.1). These categories, shown
 201 in varying shades of brown, indicate the likelihood that permafrost is present at a given location.

202

203 2.2. Data Description

204 We focused on extracting Hg measurements from environmental compartments most
 205 relevant to the terrestrial biosphere and Hg cycling models including soil, lake sediment, water,
 206 and vegetation. Water data includes observations in lakes, rivers, creeks, oceans, wetlands,
 207 ponds, and soil porewater. All observations include the following metadata: the original
 208 observation identifier if available, site name, country, sample number, date of collection,
 209 laboratory, contact name, contact email, paper identifier, latitude and longitude, measurement

210 instrument, including the analytical technique used for Hg quantification (e.g., ICP-MS, DMA,
211 CVAAS) where available, as well as total Hg concentration, total Hg measurement error, notes,
212 collector, range flag, and outlier flag. Reference lists for each observation type are provided as
213 structured .bib files in the project repository and archived with the database. A “ReadMe tab” is
214 included on Zenodo (10.5281/zenodo.18300989, concept DOI) for each database type, providing
215 detailed descriptions of all column variables and units (Olson et al., 2026). Additional metadata
216 specific to the observation type is detailed in the following paragraphs. Duplicate records across
217 sources were screened during compilation using site identifiers, geographic coordinates
218 (latitude/longitude), and reported values, and none were identified. The database may include
219 repeat sampling at the same or nearby locations across different time periods; however, repeated
220 measurements are not explicitly flagged as time series. Users can identify potential repeat
221 observations using combinations of site identifiers, geographic coordinates (latitude/longitude),
222 and sampling dates provided for each record. As a result, while the dataset supports exploratory
223 temporal analysis, it is not structured as a formal time-series dataset and should be used with
224 caution for trend analysis.

225 Soil data include available information on soil type, horizon, vegetation type, sample
226 depth, bulk density, loss-on-ignition (LOI; as a proxy for organic matter), soil organic carbon
227 content, hg-to-carbon ratio, and volumetric water content. Soil horizon and depth information
228 help distinguish surface organic layers from mineral soils, which can be markedly different in Hg
229 concentration (Lim et al., 2020). Bulk soil density and organic carbon (OC) measurements are
230 used to calculate Hg stocks, and pairing Hg with OC enables upscaling across permafrost regions
231 where OC data are widely available. ~~Loss-on-ignition (LOI)~~ provides a complementary proxy for
232 total organic matter, helping to capture variability in Hg–organic matter associations. Volumetric
233 water contents are helpful for determining MeHg production potential and possibly redox states.
234 Collectively, these parameters support assessment of Hg partitioning, transportation, and
235 transformation.

236 Lake sediment data provides a long-term archive of Hg deposition and accumulation,
237 capturing both historical and more recently derived inputs. Surface sediments are also an
238 important site of Hg methylation and are critical to understanding Hg loading to aquatic food
239 webs. Lake sediment data includes information on sampling location and context, such as soil

240 type (for porewater samples), vegetation type, location description, catchment size, wetland
241 cover, depth of sample, soil organic carbon, and Hg to carbon ratios. These metadata help us
242 interpret how Hg is retained or transported, potential Hg sources, methylation potential, and
243 deposition timeline.

244 Water data includes observations in lakes, rivers, creeks, oceans, wetlands, ponds, and
245 soil porewater. Water data also includes information on sampling location of the catchments
246 such as soil type (for porewater observations), vegetation type, site description, catchment size,
247 wetland cover, depth of sample, dissolved Hg concentration, MeHg concentration, total organic
248 carbon, dissolved organic carbon, Hg to carbon ratio, turbidity, pH, electrical conductivity,
249 alkalinity, total phosphorus, chloride, sulfate, and total dissolved solids. These water chemistry
250 measurements were included to help evaluate Hg concentrations and relevant processes in
251 aquatic systems including transformation, sources, mobility, bioavailability, binding, speciation,
252 and methylation. While multiple Hg species (e.g., dissolved Hg and methylmercury) are included
253 in the database where available, all analyses presented in this study use total Hg concentrations
254 to ensure consistency across observation types.

255 Vegetation data include scientific and common species names, vegetation type, above
256 ground biomass, and sampled components such as leaves, roots, and woody tissue, including
257 tree-ring samples that can provide temporal records of Hg accumulation (Zhang et al., 1995;
258 Kang et al., 2022). Inclusion of these variables allows for comparison of Hg concentrations
259 across plant species functional types and environmental conditions. Tree-ring data are useful for
260 understanding historical trends in atmospheric Hg, allowing for records of Hg uptake over
261 decades to centuries. This is particularly helpful in remote regions, where long-term monitoring
262 is lacking.

263 Together, these metadata and Hg measurements provide critical context for
264 understanding Hg fate, transport, and transformation across various ecosystems. By
265 standardizing and compiling these parameters, the database enables cross-site comparison, model
266 development, and process-based investigations of Hg cycling in permafrost-affected landscapes.
267 While Hg measurements and location were the primary focus of this synthesis effort, we also
268 incorporated additional environmental parameters where available to support broader application
269 and interpretation.

270

271

2.3. Data ~~Harmonization and~~ Standardization

272

273

274

275

276

277

278

279

280

281

282

The database follows a standardized file and metadata structure, with clearly defined columns, data types, and consistent formats for easy integration and use. Here, standardization refers to the alignment of data from multiple sources through unit conversion, consistent formatting, and categorization. Unit conversion was applied to ensure all measurements are reported in standard units and maintain consistency across studies. This includes ng g⁻¹ dry weight for solids (soil, lake sediment, vegetation) and ng L⁻¹ for liquids (water). When uncertainty estimates were available, they were converted to the same units. Latitude and longitude are reported in decimal degrees using the World Geodetic System 1984 (WGS 84) coordinate reference system. The database includes core identifiers such as site, location, and sample ID, collection date, laboratory name, contact person and email, sample collector information, and additional notes relevant to data interpretation.

283

284

285

286

287

288

289

290

291

292

A uniform classification standard was implemented for vegetation observations. These include vegetation type – the 12 vegetation classes defined in Virkkala et al. (2022), including boreal wetland, mixed forest, deciduous needleleaf forest, evergreen forest, deciduous broadleaf forest, sparse boreal vegetation, wetland tundra, shrub tundra, prostrate shrub tundra, graminoid tundra, and barren tundra. If the vegetation type could not be distinguished, “NA” is reported. The vegetation observations also contain a standardized “Component” column that specifies whether the observations were moss, lichen, grass, root, leaf, needle, stem, twig, bole wood, bark, or litterfall. Litterfall observations were included within the vegetation category due to their origin as plant material; however, these represent a small subset of the dataset (n = 8) and are unlikely to influence overall vegetation statistics.

293

294

295

296

297

298

299

Missing metadata, such as unreported sample depths or inferred vegetation types, were handled through reasonable assumptions based on available information and clearly flagged to document associated uncertainty and ensure transparency. Missing data are reported as “NA” for text cells and “-999” for numeric fields. No log-transformations, dry-weight recalculations, or normalization procedures were performed. Outlier and range thresholds were applied only as quality-control flags (Sect. 2.4) and did not modify original data values. A complete description of variables and units for each observation type is provided in the metadata file through the

Formatted: Font: (Default) Times New Roman

Formatted: Normal, Indent: Left: 0", First line: 0.5"

300 project repository. The implications of these assumptions, variable uncertainty reporting, and
301 methodological heterogeneity across studies are further evaluated through uncertainty indicators
302 and validation checks described in Sect. 2.4.

303 2.4 Uncertainty and Quality Control

305 Uncertainty in the PermHg database arises primarily from heterogeneity in sampling
306 methods, analytical techniques, reporting standards, and metadata completeness across
307 contributing studies. Where available, analytical method information is included to provide
308 transparency on measurement techniques (e.g., ICP-MS, CVAAS, DMA) and to allow users to
309 consider potential differences in detection limits and analytical precision across studies. Because
310 the database compiles previously published observations rather than generating new
311 measurements, uncertainty characterization focuses on identifying potential sources of variability
312 and providing transparent indicators to support cautious interpretation, rather than re-evaluating
313 analytical accuracy.

314 Cross-study consistency and potential uncertainty were assessed using range checks and
315 statistical outlier flagging. Range flags are numerical indicators assigned to a data point based on
316 whether the values fall outside predefined conservative screening thresholds. For this database,
317 we use a conservative upper bound of 500 ng g⁻¹ for soil, lake sediment, and vegetation
318 observations and 100 ng L⁻¹ for water observations. Any observation above these values was
319 assigned a “1” in the range flag column to indicate that it surpassed the screening threshold.
320 Observations that fell below these range flags were assigned a “0”. The thresholds were selected
321 based on published ranges reported in global and regional studies and were intended to represent
322 conservative screening values broadly consistent with concentrations observed in many non-
323 impacted systems (Mei Lu et al., 2016; Olson et al., 2022; Wohlgemuth et al., 2022). Any outlier
324 exceeding three times the interquartile range (difference between first and third quartile) was
325 flagged and assigned a “1”. All other values not exceeding 3xIQR were assigned “0”. These
326 flags are intended as screening indicators rather than measures of analytical uncertainty; for
327 example, a value assigned a range flag of “1” exceeds conservative screening thresholds, while
328 an outlier flag of “1” indicates values exceeding three times the interquartile range. These

Formatted: Font: (Default) Times New Roman, Bold

Formatted: Normal, Indent: Left: 0", First line: 0.5",
Line spacing: 1.5 lines

Formatted: Font: (Default) Times New Roman, Bold

Formatted: Outline numbered + Level: 2 + Numbering
Style: 1, 2, 3, ... + Start at: 4 + Alignment: Left + Aligned
at: 0.5" + Indent at: 0.75"

329 indicators do not imply data removal or correction but are provided to support user
330 interpretation.

331 Analytical uncertainty was included for total Hg, MeHg, dissolved Hg, total organic
332 carbon, dissolved organic carbon, soil organic carbon, Hg to carbon ratio, volumetric water
333 content, and bulk density when such information was reported in the source studies. However,
334 uncertainty reporting was inconsistent across publications, and many observations lack explicit
335 error estimates or detection limits. As a result, uncertainty cannot be uniformly quantified across
336 the entire dataset. Analytical uncertainties were therefore retained as reported in the original
337 studies and were not aggregated or standardized across the dataset. To address this limitation,
338 qualitative uncertainty information and assumptions made during data extraction (e.g., inferred
339 coordinates or sample depths) were documented in a notes field associated with each observation
340 type to provide users with additional context regarding potential sources of uncertainty or bias.

341 **2.5 Data Analysis**

342 We used several tools to analyze the PermHg database. To visualize the spatial distribution
343 and density of Hg observations globally, we used point clustering in ArcGIS Pro to generate
344 plots where observations were aggregated into circular clusters of varying size, with each circle
345 scaled to represent the number of observations within a given area. Boxplots were generated
346 using Python (version 3.13.3) with the Seaborn and Matplotlib libraries to visualize the
347 distribution of Hg concentrations across observation types and regions. Microsoft Excel was
348 used to generate column charts and explore the distribution of Hg concentrations across
349 observation types. Summary statistics, including count, mean, geometric mean, standard
350 deviation, first quartile (Q1), and third quartile (Q3), were calculated using built-in Excel
351 functions. These built-in functions provided a preliminary assessment of central tendency,
352 spread, and skewness within each observation type.

353 **3. Validation**

354 Validation of the PermHg database focuses on assessing internal coherence and
355 plausibility of the compiled observations rather than independent verification of individual
356 measurements. As the database aggregates previously published data, validation is based on
357 consistency across studies, agreement with established environmental patterns, and transparent
358 documentation of uncertainty and quality indicators (Sects. 2.3–2.4).

Formatted: Font: (Default) Times New Roman
Formatted: Normal, Indent: First line: 0.25", No
bullets or numbering

359 Across observation types and geographic subsets, the compiled data exhibit internally
360 consistent and environmentally plausible patterns. Summary statistics and distributional analyses
361 (Sect. 4; Figs. 2 and 4) show relative mercury concentrations among lake sediment, soil,
362 vegetation, and water that align with well-established mercury partitioning and accumulation
363 processes in terrestrial and aquatic systems (Section 2.4). No systematic contradictions or study-
364 level anomalies were identified that would indicate errors arising from data compilation or
365 standardization.

366 Validation does not assess the analytical accuracy of individual measurements, which
367 remains the responsibility of the original studies. Instead, the combination of standardized data
368 structures, uncertainty indicators, range and outlier flags, and cross-study consistency supports
369 the use of the PermHg database for synthesis, comparative analyses, and model applications,
370 provided users account for documented limitations and uncertainty from each respective study.

371 4. Results

372 4.1. Data Summary

373 **Table 1** below details the observation count, median, geometric mean, standard
374 deviation, and upper and lower quartiles for each sample medium. These values highlight the
375 variability and distribution of Hg concentrations within each medium. A total of ~~30+~~ papers were
376 included for the vegetation observations, ~~four~~ ~~five~~ papers for the lake sediment observations, ~~17~~
377 ~~28~~ papers for the soil observations, and ~~10+~~ papers for the water observations. A small subset of
378 unpublished data was included for some observation types, comprising approximately 68
379 sediment observations and 75 water observations. The studies included in the database are
380 summarized in a table, with full citation details provided in Zenodo under the [concept](https://doi.org/10.5281/zenodo.18300989)
381 [DOI:10.5281/zenodo.18300989](https://doi.org/10.5281/zenodo.18300989) (Olson et al., 2026).

382 **Table 1.** Summary statistics of Hg observations in permafrost-dominated regions including lake sediment
383 (ng g⁻¹), soil (ng g⁻¹), vegetation (ng g⁻¹), and water (ng L⁻¹, ~~total Hg~~). The minimum, 25th percentile,
384 median, 75th percentile, maximum, geometric mean, standard deviation, and count are included for each
385 medium type.

Formatted: Font: (Default) Times New Roman

Formatted: Font: (Default) Times New Roman

Formatted: Font: (Default) Times New Roman

Formatted: Not Highlight

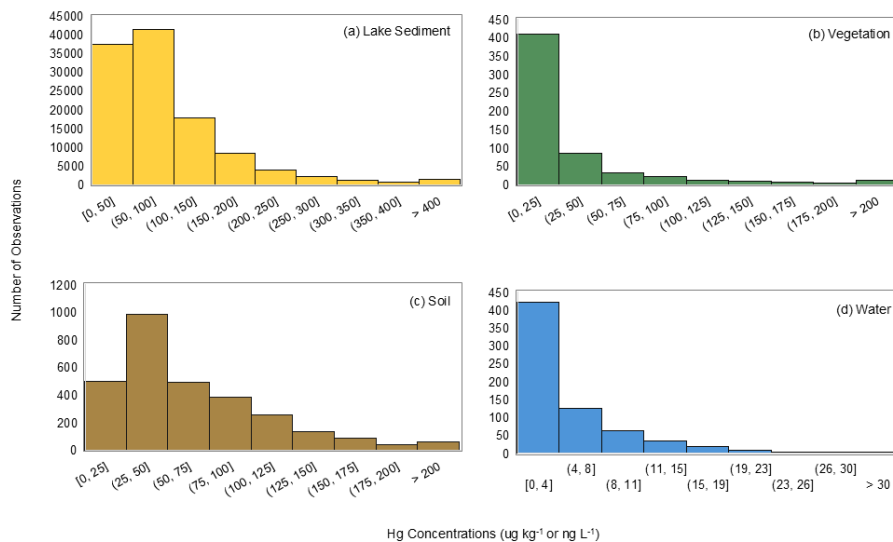
Commented [Ui1]: 5 instead of five ?

Formatted: Not Highlight

Formatted: Not Highlight

	Lake Sediment (ng g ⁻¹)	Soil (ng g ⁻¹)	Vegetation (ng g ⁻¹)	Water (ng L ⁻¹)
Minimum	1	1	1	0.0
25th Percentile	45	32	9	1.5
Median	70	50	15	2.5
75th Percentile	116	90	33	5.9
Maximum	9820	503	400	32.6
Geometric Mean	71	48	17	2.0
Standard Deviation	118	48	51	5.0
Count	113613	2923	590	676

386
 387 Mercury concentrations across the four observation types—lake sediment, soil, vegetation, and
 388 water—displayed predominantly left positively-skewed distributions (**Fig. 2**). Lake sediment and
 389 soil observations showed higher median Hg concentrations compared to vegetation and water,
 390 consistent with their roles as primary Hg reservoirs. Vegetation exhibited the lowest
 391 concentrations overall, while water Hg concentrations, though generally low, spanned a
 392 relatively wide range. The skewness in all matrices highlights that low-to-moderate
 393 concentration observations are more common than extreme high values.



394
 395 **Figure 2.** Histogram distributions of mercury concentrations in (a) lake sediment, (b) vegetation, (c) soil,
 396 and (d) water (total Hg). All matrices show left positively-skewed distributions, with lake sediment and soil

397 exhibiting higher median concentrations than vegetation and water. Water concentrations (total Hg) are
398 plotted on a separate y-axis scale to accommodate lower values relative to solid matrices.

399
400 **Figure 1** shows the geographic distribution of data points on a global map, illustrating
401 the spatial spread of measurements across the study region. Circle size and numbers within the
402 circles show observation density. Lake sediment observations are largely concentrated in
403 Canada, particularly towards the eastern side of the country. Some lake sediment observations
404 also occurred in the Canadian Arctic Archipelago and northern Russia. Vegetation observations
405 are concentrated in central Alaska, the Tibetan Plateau, and northern Europe. Some vegetation
406 observations are also visible in northern China, Greenland, Russia, and Canada. Soil
407 observations are highly concentrated in Alaska, the Tibetan Plateau, western Canada and
408 northern Europe, with clusters also existing in western Russia and the Rocky Mountains of the
409 United States. Water observations were the sparsest, with sampling clustered in the north slope
410 of Alaska and along major Arctic Rivers—the Ob, Mackenzie, Yukon, Lena, and Kolyma. Some
411 water observations are also present in the Hudson Bay of Canada.

412 To quantitatively assess spatial representativeness, **Table 2** summarizes sampling density
413 as the number of observations per 10⁶ km² of permafrost area by region and observation type.
414 Permafrost area is defined following Gruber (2012) as land area actually underlain by
415 permafrost. Sampling density varies substantially across regions, with North America exhibiting
416 the highest observation density across most media (e.g., 70 water and 193 soil observations per
417 10⁶ km²), while Eurasia, represented by Russia, remains comparatively underrepresented (16
418 water and 21 soil observations per 10⁶ km²). Northern Europe and the Tibetan Plateau show
419 intermediate sampling densities, with variability depending on observation type (e.g., high soil
420 density in northern Europe but limited water observations). Differences among environmental
421 media are also evident. Soil and vegetation observations are relatively well distributed, whereas
422 water observations remain sparse across all regions. Lake sediment observations show the
423 highest apparent sampling densities, particularly in North America (15,825 observations per 10⁶
424 km²); however, these values reflect multiple samples collected at individual sites (e.g., sediment
425 cores) and therefore are not directly comparable to other media in terms of spatial coverage.

426 **Table 2.** Sampling density (observations per 10⁶ km² of permafrost area) by region and medium.

Formatted: Font: Bold

Formatted: Superscript

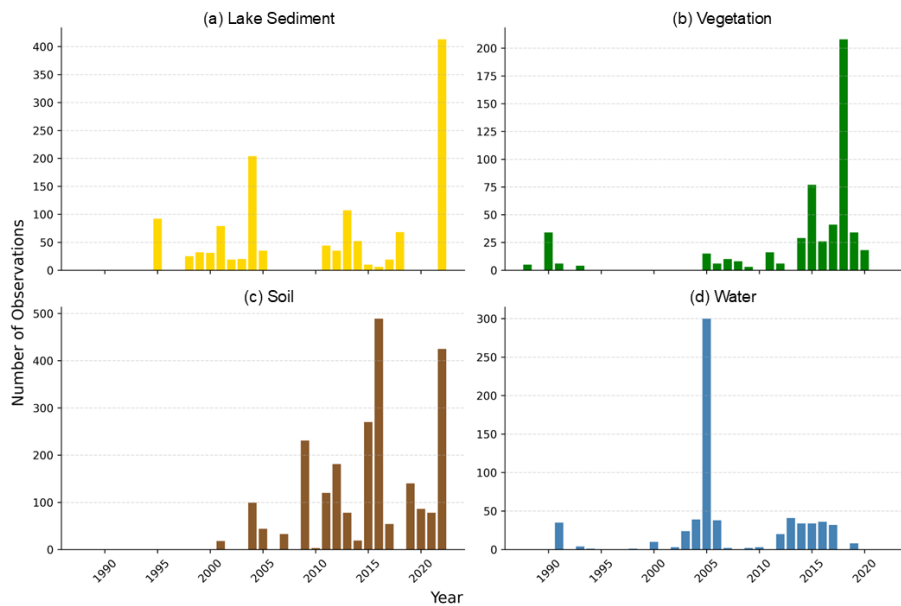
Formatted: Superscript

	Area (10 ⁶ km ²)	Water	Soil	Lake Sediment	Vegetation
North America	7.16	70	193	15825	26
Northern Europe	0.14	-	3629	741	357
Eurasia (Russia)	10.97	16	21	31	0
Tibetan Plateau	2.07	-	305	0	84

Formatted: Indent: First line: 0"

427

428 The temporal distribution of Hg observations in the PermHg database is shown in **Fig. 3**,
 429 highlighting the years in which samples were collected for each observation type. Lake sediment
 430 observations span from 1995 to 2022, with notable peaks in sampling effort in 2004 and again in
 431 2022. Soil observations cover the period from 2001 to 2022, with steadily increasing sample
 432 counts that peak in 2017 and 2022; 81% of these records include a collection date. Vegetation
 433 observations had the longest temporal range, spanning from 1988 to 2020, with a prominent peak
 434 in 2018. Nearly all vegetation observations (94%) are associated with a specific year. Water
 435 observations were collected between 1991 and ~~2017~~2019, with a sharp spike in 2005 that far
 436 exceeds sampling effort in other years. These records are the most complete in terms of temporal
 437 metadata, with over 98% including a collection date.



438

439 **Figure 3.** 2D column chart showing the number of observations collected over time for (a) lake sediment,
440 (b) vegetation, (c) soil, and (d) water Hg observations in the PermHg database.

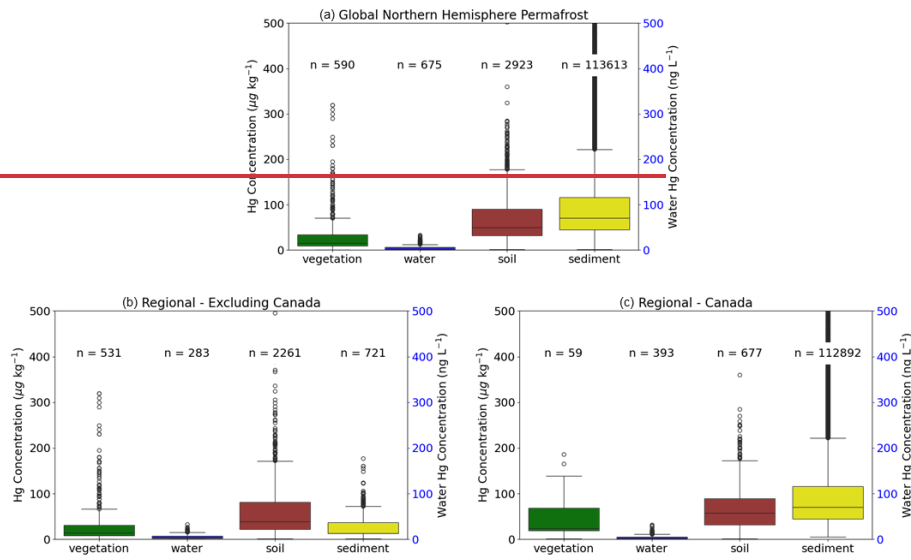
442 4.2. Data Analysis

443 Overall, the observation distribution is heavily biased by both matrix type and geographic
444 region. Lake sediment observations account for over 90% of all data points, highlighting a strong
445 skew toward this medium relative to soil, vegetation, and water. Geographically, the majority of
446 observations exist in Canada and across the Western Hemisphere, with Canada alone
447 contributing over 90% of the total observations. In contrast, there are significant spatial gaps in
448 Eurasia, particularly across Russia and northern China. This uneven distribution may reflect
449 differences in research funding, accessibility, existing monitoring programs, and the composition
450 of author teams. In addition, data availability may be limited in some countries where
451 observations are not routinely shared publicly or translated into English. As a result, care should
452 be taken when extrapolating trends across under-represented regions or observation types. ~~As a~~
453 ~~result, care should be taken when extrapolating trends across under-represented regions or~~
454 ~~observation types.~~

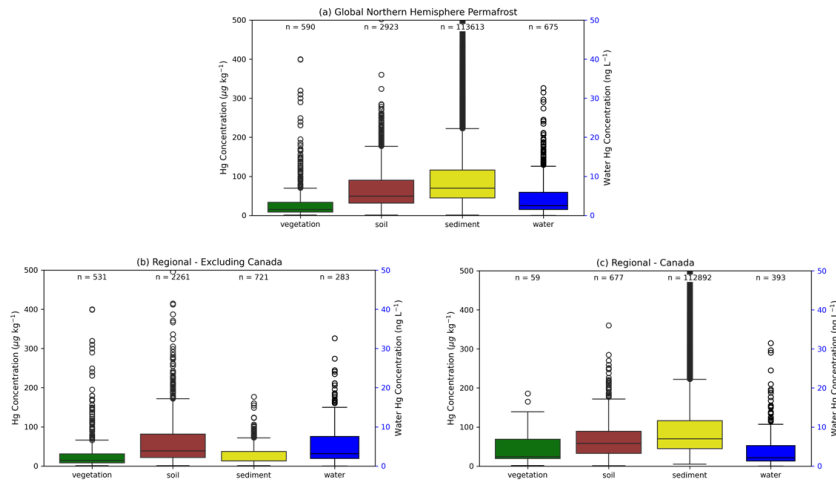
455 Boxplots were used to visualize Hg concentration distributions across lake sediment, soil,
456 vegetation, and water observations at both global and regional scales (Fig. 4). Across all subsets,
457 lake sediment exhibited the highest median concentrations, followed by soil, with vegetation
458 consistently showing the lowest values. Mercury concentrations in water are reported in ng L^{-1}
459 and are plotted on a secondary y-axis to account for the differing units, while concentrations in
460 sediment, soil, and vegetation are reported in ug kg^{-1} dry weight. Across both global and
461 Canadian subsets, Hg concentrations follow a consistent pattern by matrix: lake sediment > soil
462 > vegetation ~~→ water~~. In contrast, observations from all other countries followed the order soil >
463 lake sediment > vegetation ~~→ water~~, which may be a result of the reversal of sample size for lake
464 sediment and soil observations. The exclusion of Canada in this comparison is intentional, as
465 Canada contains the vast majority of lake sediment observations and accounts for over 90% of
466 the total dataset, with sample sizes differing by orders of magnitude across matrices (Fig. 4; e.g.,
467 sediment n = 113,613 vs. vegetation n = 590). The shift in ordering outside of Canada highlights
468 the sensitivity of cross-matrix comparisons to dataset composition and uneven sampling.

Formatted: Font: Bold

469



470



471 **Figure 4.** Boxplots of Hg concentrations across lake sediment, soil, vegetation and water observation
472 types for (a) Global Northern Hemisphere Permafrost, (b) Regional – Excluding Canada, and (c) Regional
473 – Canada. T-tests within each grouping showed statistically significant differences among most
474 observation types, except between vegetation and sediment for countries outside Canada. Water Hg

475 concentrations (total Hg) are shown on a separate y-axis due to differing units (ng L⁻¹ vs. µg kg⁻¹ dry
476 weight) and are not directly comparable to the other matrices.

477 We used two sample t-tests to assess whether differences in Hg concentrations between pairs
478 of observation types were statistically significant, considering only two groups at a time.
479 Mercury concentrations across all observation types were positively skewed, with most values
480 being low to moderate in concentration and a small number of high values elevating the mean. F-
481 tests were first used to assess the equality of variances before choosing a two-sample t-test.
482 Variances were unequal for all comparisons except between vegetation and soil (p=0.013
483 globally; p=0.071 within Canadian observations), so Welch's t-test (assuming unequal variances)
484 was used in most cases. Both global and regional analyses revealed statistically significant
485 differences in Hg concentrations among observation types, with the exception noted above.
486 Overall, these results ~~reinforce generally support the general the~~ pattern of lake sediment > soil >
487 vegetation, although, as noted above, this ordering is sensitive to dataset composition. This
488 hierarchy is broadly consistent with observations from ~~neonsistent with findings from non-~~
489 ~~permafrost regions. This hierarchy is consistent with observations from other landscape types~~
490 ~~(i.e., non-cold regions)~~, suggesting that these concentration patterns may reflect general
491 biogeochemical processes rather than being unique to permafrost-affected environments
492 (Gworek et al., 2016, 2020).

493

494 5. Discussion

495 The PermHg database should be useful to a wide audience including researchers and
496 scientists, policymakers, regulators, environmental managers, educators, and the public. ~~With~~
497 ~~regard to~~ Regarding scientific research, this database may be useful for a ~~wide variety broad~~
498 range of studies including environmental fate and transport, contaminant modeling, risk
499 assessment, climate change impacts, remote sensing, earth system modeling, ecotoxicology, and
500 food web studies. Potential applications include but are not limited to calibration and validation
501 of atmospheric and terrestrial models, future global Hg budget studies, identifying global trends
502 and regional hotspots, biogeochemical controls, and assessing human and ecosystem health risks
503 from Hg exposure pathways. The database is also recommended for use in spatial analysis by

Formatted: paragraph, Indent: Left: 0", Line spacing:
1.5 lines, Font Alignment: Baseline

504 providing empirical constraints for satellite-based observations and synthesis reviews to support
505 integrated Hg research in permafrost regions. PermHg provides a baseline for future observations
506 and for tracking Hg levels and trends over time. It can also serve as a valuable guide for research
507 teams working in Arctic regions, helping identify where new measurements could have the most
508 impact and inform future field collection efforts.

509 Outside of the scientific research community, this database can help assess whether Hg
510 concentrations exceed regional regulatory limits or advisories and support compliance with
511 international agreements like the Minamata Convention on Mercury. PermHg may aid in
512 identifying contaminated sites or regions needing additional intervention or monitoring and help
513 guide additional sampling or mitigation based on spatial and observation type gaps. The database
514 may also support baseline environmental studies for infrastructure development or resource
515 extraction. We hope this database will serve the public interest through real-world examples of
516 pollutant pathways and highlight global and local Hg concerns, especially in Arctic or
517 Indigenous communities where some country foods are at risk of elevated Hg concentrations
518 (Arctic Monitoring and Assessment Programme, 2022).

519 Despite these broad applications, several limitations should be considered when using the
520 database~~Due to methodological heterogeneity, the database has several limitations that should be~~
521 considered in future analysis and applications. These include uneven spatial and temporal
522 coverage, with sampling efforts concentrated in certain regions (e.g., Canada and the Western
523 Hemisphere) and time periods, leaving notable gaps in underrepresented areas such as Russia or
524 China. Temporal coverage of observations is sparse before the 1990s, and some observation
525 types include extended gaps in coverage (e.g., 3-5 years). A significant portion of the
526 measurements lack reported uncertainty or quality assurance information, limiting the ability to
527 assess data precision and comparability across studies. Variation in sampling methods, analytical
528 techniques, temporal heterogeneity in sampling period (e.g., day, month, season), and detection
529 limits may also contribute to inconsistencies and should be accounted for when interpreting or
530 modeling Hg in permafrost regions.

531 The PermHg database is best suited for large-scale synthesis, model calibration and
532 evaluation, and identification of broad spatial patterns in Hg distribution across permafrost
533 regions. It may be less suitable for analyses requiring balanced representation across

534 environmental media (e.g., direct comparisons among soil, vegetation, and aquatic systems),
535 fine-scale process studies, or site-specific assessments of Hg cycling. In particular, the
536 dominance of lake sediment observations and geographic clustering of data may limit its
537 applicability for tightly coupled vegetation–soil interactions, or studies requiring co-located
538 multi-compartment measurements. Users are therefore encouraged to subset the data and
539 evaluate representativeness relative to their specific research question. Future database
540 development could also incorporate additional Hg characterization metrics, including Hg
541 speciation, organic versus inorganic fractions, bioavailable Hg pools, and stable isotope
542 measurements where available, to support more process-based investigations of Hg cycling in
543 permafrost systems.

544 ~~This database can serve as a valuable guide for research teams working in Arctic regions,~~
545 ~~helping identify where new measurements could have the most impact and inform future field~~
546 ~~collection efforts. As the first integrated Hg database for measurements in permafrost regions, it~~
547 ~~provides a baseline for future observations and for tracking Hg levels and trends over time. To~~
548 support long-term growth and community engagement, the database is ~~hosted on a GitHub~~
549 ~~repository linked to Zenodo (see Sect. 5)~~maintained as an open, version-controlled database with
550 permanent archiving and community contribution mechanisms (see Sect. 6), enabling version-
551 controlled contributions, transparent issue tracking, and permanent archiving. A contribution
552 guide ~~will~~provides instructions for submitting new data and ensuring consistent quality control.
553 Ongoing oversight could be coordinated through a lightweight advisory mechanism, potentially
554 under the International Permafrost Association or Arctic Monitoring and Assessment
555 Programme, to maintain data quality and guide updates. By facilitating community-driven
556 expansion in a structured, open-access format, the PermHg database can contribute to
557 international Hg monitoring efforts, including supporting effectiveness evaluation under the
558 Minamata Convention.

559 **6. Data Availability**

560 In alignment with open science principles, the PermHg dataset and its accompanying
561 documentation are hosted on GitHub (<https://github.com/IGE-mercury/PermHg>) and archived
562 ~~on.~~ The PermHg database is archived on Zenodo under the concept DOI
563 10.5281/zenodo.18300989, which links all released versions of the dataset. The specific version

Formatted: Indent: First line: 0.5"

564 used and described in this manuscript is archived as 10.5281/zenodo.18483492 (Olson et al.,
565 2026). Users are encouraged to cite both this data paper and the appropriate Zenodo DOI when
566 using the dataset.

567 _____
568 GitHub serves as the platform for community contributions and version control, with updates
569 tracked and periodic releases archived on Zenodo under unique DOIs to ensure reproducibility
570 and long-term accessibility. Contributions of new data can be submitted through the repository
571 workflow described in the project documentation on GitHub or via email. ~~Users who wish to~~
572 ~~propose modifications, additions, or corrections to the data or documentation should follow the~~
573 ~~contribution workflow outlined in the repository's README.md file. This involves creating a~~
574 ~~personal copy of the repository, implementing changes, and submitting them for review via a~~
575 ~~pull request. Once approved, changes are merged into the main branch, and periodic updates are~~
576 ~~released on Zenodo to reflect significant additions or improvements.~~

577 ~~For users unfamiliar with GitHub, data submissions are also welcome via email (permhg@univ-~~
578 ~~grenoble-alpes.fr). Our aim is to foster an open, evolving database that grows through~~
579 ~~collaborative input, thereby supporting transparent and reproducible research.~~ Long-term
580 stewardship of the database is maintained by the authors, with ongoing updates supported
581 through community contributions and collaborative oversight (Section 5).

582 The database includes a wide range of metadata fields that allow users to filter
583 observations based on data completeness and quality. Key attributes such as geographic
584 coordinates, sampling date, laboratory information, and analytical uncertainty are available for
585 many records, although completeness varies by observation type (see metadata documentation).
586 For example, soil-specific variables such as horizon and organic carbon content are included
587 where reported, while water and vegetation datasets include additional parameters relevant to
588 those systems. Users are therefore encouraged to subset the dataset based on the availability of
589 required metadata for their specific application.

590 A subset of the soil permafrost mercury observations included in the PermHg compilation
591 (n = 1,752 records) originates from a curated permafrost mercury database hosted by the Bolin

Formatted: Indent: First line: 0.5"

592 [Centre for Climate Research. These data are archived separately and will be cited via a dedicated](https://doi.org/10.17043/azaroff-2026-permafrost-mercury-1)
593 [digital object identifier \(https://doi.org/10.17043/azaroff-2026-permafrost-mercury-1\).](https://doi.org/10.17043/azaroff-2026-permafrost-mercury-1)

594 7. Conclusion

595 This study compiles one of the most comprehensive publicly available database of Hg
596 concentrations in permafrost-affected environments to date. PermHg addresses a longstanding
597 data gap of Hg concentrations in Arctic and sub-Arctic regions, allowing the opportunity to
598 analyze spatial patterns, assess climate change impacts, and model biogeochemical cycling at
599 regional to global scales. This database can inform monitoring programs, support regulatory
600 frameworks like the Minamata Convention, and guide international efforts to mitigate Hg
601 exposure in northern communities.

602 The development of this database was made possible through collaborative contributions
603 from a broad scientific community and is intended to support researchers, decision makers, and
604 the public. Its standardized format supports integration into Earth system models, remote
605 sensing products, and other geospatial datasets to track and predict Hg behavior in response to
606 environmental change. This database provides a critical foundation for future integrated Hg
607 research across high-latitude ecosystems.

608 The database is archived and accessible through a GitHub repository linked to Zenodo
609 ([concept DOI:10.5281/zenodo.18300989](https://doi.org/10.5281/zenodo.18300989)), [supporting continued development, citation, and reuse](#)
610 ([Olson et al., 2026](#)). While current data coverage is uneven, PermHg highlights key areas where
611 future field sampling and monitoring could have the greatest impact, including Russia and China.
612 The incorporation of additional soil, vegetation, and water observations will also be essential to
613 providing a more balanced database across observation types. As permafrost regions continue to
614 warm, this database lays the foundation for more interdisciplinary investigations of Hg cycling
615 and implications to human and ecosystem health.

616 8. Author contribution

617 CLO, KS, AA, LSLT, and DO led the conceptualization of the study. CLO prepared the original
618 draft of the manuscript. All authors contributed data to the PermHg database and participated in
619 data curation and quality control. CLO and KS acquired financial support for the project. EJ,
620 CLO, and HA contributed to database curation, including preparation of metadata and uploading

621 data products to GitHub and Zenodo. All authors reviewed and edited the manuscript and
622 approved the final version.

623 9. Competing Interests

624 The authors declare that they have no conflict of interest.

625 10. Acknowledgments

626 Financial support for this work was provided by the International Permafrost Association Action
627 Group Award in 2024 ([https://www.permafrost.org/group/permhg-a-global-database-of-mercury-
628 concentrations-in-permafrost-and-active-layer-soils/](https://www.permafrost.org/group/permhg-a-global-database-of-mercury-concentrations-in-permafrost-and-active-layer-soils/)). LS, EJ, and HA received funding from the
629 ANR ATOX project (ANR-24-CE01-7616). [GH acknowledges funding support from the
630 Nunataryuk and ILLUQ projects under the European Union's Horizon Europe Research and
631 Innovation Programme and the Swedish Research Council VR \(grant no. 2022-04839\)](#). The
632 authors used ChatGPT (OpenAI, GPT-5-mini) to assist with language editing and clarity of the
633 manuscript. All scientific content, interpretations, and data were authored and verified by the
634 authors.

635

636 11. References

- 637 Basu, N., Abass, K., Dietz, R., Krümmel, E., Rautio, A., and Weihe, P.: The impact of mercury
638 contamination on human health in the Arctic: A state of the science review, *Science of The Total
639 Environment*, 831, 154793, <https://doi.org/10.1016/j.scitotenv.2022.154793>, 2022.
- 640 Chételat, J., McKinney, M. A., Amyot, M., Dastoor, A., Douglas, T. A., Heimbürger-Boavida,
641 L.-E., Kirk, J., Kahilainen, K. K., Outridge, P. M., Pelletier, N., Skov, H., St. Pierre, K.,
642 Vuorenmaa, J., and Wang, F.: Climate change and mercury in the Arctic: Abiotic interactions,
643 *Science of The Total Environment*, 824, 153715,
644 <https://doi.org/10.1016/j.scitotenv.2022.153715>, 2022.
- 645 Dastoor, A., Angot, H., Bieser, J., Christensen, J. H., Douglas, T. A., Heimbürger-Boavida, L.-
646 E., Jiskra, M., Mason, R. P., McLagan, D. S., Obrist, D., Outridge, P. M., Petrova, M. V.,
647 Ryjkov, A., St. Pierre, K. A., Schartup, A. T., Soerensen, A. L., Toyota, K., Travníkov, O.,
648 Wilson, S. J., and Zdanowicz, C.: Arctic mercury cycling, *Nature Reviews Earth &
649 Environment*, 3, 270–286, <https://doi.org/10.1038/s43017-022-00269-w>, 2022.
- 650 Fabre, C., Sonke, J. E., Tananaev, N., and Teisserenc, R.: Organic carbon and mercury exports
651 from pan-Arctic rivers in a thawing permafrost context – A review, *Science of The Total
652 Environment*, 954, 176713, <https://doi.org/10.1016/j.scitotenv.2024.176713>, 2024.

653 [Fitzgerald, W. F., & Lamborg, C. H. \(2014\). 11.4 - Geochemistry of Mercury in the](#)
654 [Environment. In *Treatise on Geochemistry* \(pp. 91–129\). Elsevier Ltd. <https://doi->](#)
655 [org.colorado.idm.oclc.org/10.1016/B978-0-08-095975-7.00904-9](https://doi.org/colorado.idm.oclc.org/10.1016/B978-0-08-095975-7.00904-9)

656 Gartler, S., Scheer, J., Meyer, A., Abass, K., Bartsch, A., Doloisio, N., Falardeau, J., Hugelius,
657 G., Irrgang, A., Haukur Ingimundarson, J., Jungsberg, L., Lantuit, H., Nymand Larsen, J., Lodi,
658 R., Martin, V. S., Mercer, L., Nielsen, D., Overduin, P., Povoroznyuk, O., Rautio, A.,
659 Schweitzer, P., Speetjens, N. J., Tomaškovičová, S., Timlin, U., Vanderlinden, J.-P., Vonk, J.,
660 Westerveld, L., and Ingeman-Nielsen, T.: A transdisciplinary, comparative analysis reveals key
661 risks from Arctic permafrost thaw, *Communications Earth & Environment*, 6, 21,
662 <https://doi.org/10.1038/s43247-024-01883-w>, 2025.

663 Giest, F. P., Jenrich, M., Grosse, G., Jones, B. M., Mangelsdorf, K., Windirsch, T., and Strauss,
664 J.: Organic carbon, mercury, and sediment characteristics along a land–shore transect in Arctic
665 Alaska., *Biogeosciences*, 22, 2871–2887, <https://doi.org/10.5194/bg-22-2871-2025>, 2025.

666 [Gruber, S. \(2012\). Derivation and analysis of a high-resolution estimate of global permafrost](#)
667 [zonation. *The Cryosphere*, 6\(1\), 221.](#)

668 Gworek, B., Bemowska-Kalabun, O., Kijenska, M., and Wrzosek-Jakubowska, J.: Mercury in
669 Marine and Oceanic Waters-a Review, *WATER AIR AND SOIL POLLUTION*, 227,
670 <https://doi.org/10.1007/s11270-016-3060-3>, 2016.

671 Gworek, B., Dmuchowski, W., and Baczevska-Dąbrowska, A. H.: Mercury in the terrestrial
672 environment: a review, *Environmental Sciences Europe*, 32, 128, [https://doi.org/10.1186/s12302-](https://doi.org/10.1186/s12302-020-00401-x)
673 [020-00401-x](https://doi.org/10.1186/s12302-020-00401-x), 2020.

674 Horsburgh, J. S., Tarboton, D. G., Piasecki, M., Maidment, D. R., Zaslavsky, I., Valentine, D.,
675 and Whitenack, T.: An integrated system for publishing environmental observations data,
676 *Environmental Modelling & Software*, 24, 879–888,
677 <https://doi.org/10.1016/j.envsoft.2009.01.002>, 2009.

678 Jonsson, S., Mastromonaco, M. N., Wang, F., Bravo, A. G., Cairns, W. R. L., Chételat, J.,
679 Douglas, T. A., Lescord, G., Ukonmaanaho, L., and Heimbürger-Boavida, L.-E.: Arctic
680 methylmercury cycling, *Science of The Total Environment*, 850, 157445,
681 <https://doi.org/10.1016/j.scitotenv.2022.157445>, 2022.

682 Kang, H., Liu, X., Guo, J., Zhang, Q., Wang, Y., Huang, J., Xu, G., Wu, G., Ge, W., and Kang,
683 S.: Long-term mercury variations in tree rings of the permafrost forest, northeastern China, *Sci.*
684 *China Earth Sci.*, 65, 1328–1338, <https://doi.org/10.1007/s11430-021-9886-1>, 2022.

685 Lim, A. G., Jiskra, M., Sonke, J. E., Loiko, S. V., Kosykh, N., and Pokrovsky, O. S.: A revised
686 pan-Arctic permafrost soil Hg pool based on Western Siberian peat Hg and carbon observations.,
687 *Biogeosciences*, 17, 3083–3097, <https://doi.org/10.5194/bg-17-3083-2020>, 2020.

Formatted: Normal

Formatted: Font: (Default) +Body (Aptos)

Formatted: Font: (Default) Times New Roman

Formatted: Normal

688 MacMillan, G. A., Girard, C., Chételat, J., Laurion, I., and Amyot, M.: High Methylmercury in
689 Arctic and Subarctic Ponds is Related to Nutrient Levels in the Warming Eastern Canadian
690 Arctic, *Environ. Sci. Technol.*, 49, 7743–7753, <https://doi.org/10.1021/acs.est.5b00763>, 2015.

691 Mei Lu, Wang Xun, Feng Xinbin, and Luo Ji: Spatial distribution and source/ sink characteristic
692 of mercury in the water samples from the Mt. Gongga area in the Tibetan Plateau, *Huanjing*
693 *Huaxue-Environmental Chemistry*, 35, 1549–1556, [https://doi.org/10.7524/j.issn.0254-](https://doi.org/10.7524/j.issn.0254-6108.2016.08.2015122301)
694 6108.2016.08.2015122301, 2016.

695 Obrist, D., Agnan, Y., Jiskra, M., Olson, C. L., Colegrove, D. P., Hueber, J., Moore, C. W.,
696 Sonke, J. E., and Helmig, D.: Tundra uptake of atmospheric elemental mercury drives Arctic
697 mercury pollution, *Nature*, 547, 201–204, <https://doi.org/10.1038/nature22997>, 2017.

698 Obu, J., Westermann, S., Bartsch, A., Berdnikov, N., Christiansen, H. H., Dashtseren, A.,
699 Delaloye, R., Elberling, B., Etzelmüller, B., Kholodov, A., Khomutov, A., Kääh, A., Leibman,
700 M. O., Lewkowicz, A. G., Panda, S. K., Romanovsky, V., Way, R. G., Westergaard-Nielsen, A.,
701 Wu, T., Yamkhin, J., and Zou, D.: Northern Hemisphere permafrost map based on TTOP
702 modelling for 2000–2016 at 1 km2 scale, *Earth-science reviews*, 299–316, 2019a.

703 Obu, J., Westermann, S., Bartsch, A., Berdnikov, N., Christiansen, H., Dashtseren, A., Delaloye,
704 R., Elberling, B., Etzelmüller, B., Kholodov, A., Khomutov, A., Kääh, A., Leibman, M.,
705 Lewkowicz, A., Panda, S., Romanovsky, V., Way, R., Westergaard-Nielsen, A., Wu, T.,
706 Yamkhin, J., and Zou, D.: Northern Hemisphere permafrost map based on TTOP modelling for
707 2000–2016 at 1 km2 scale, *EARTH-SCIENCE REVIEWS*, 193, 299–316,
708 <https://doi.org/10.1016/j.earscirev.2019.04.023>, 2019b.

709 Olson, C.I., Geyman, B., Thackray, C., Krabbenhoft, D., Tate, M., Sunderland, E., and Driscoll,
710 C.: Mercury in soils of the conterminous United States: patterns and pools, *ENVIRONMENTAL*
711 *RESEARCH LETTERS*, 17, <https://doi.org/10.1088/1748-9326/ac79c2>, 2022.

712 Olson, C., Jiskra, M., Biester, H., Chow, J., and Obrist, D.: Mercury in Active-Layer Tundra
713 Soils of Alaska: Concentrations, Pools, Origins, and Spatial Distribution, *Global Biogeochemical*
714 *Cycles*, 32, 1058–1073, <https://doi.org/10.1029/2017GB005840>, 2018.

715 Olson, C. L., Jiskra, M., Sonke, J. E., and Obrist, D.: Mercury in tundra vegetation of Alaska:
716 Spatial and temporal dynamics and stable isotope patterns, *Science of the total environment*,
717 1502–1512, 2019.

718 Olson, C., Schaefer, K., Azaroff, A., Angot, H., Douglas, T. A., Fahnestock, M. F., Haugk, C.,
719 Hugelius, G., Jahangir, E., Jonsson, S., Kirkwood, A., Korosi, J., Nasr, M., Olefeldt, D., Olson,
720 C., Sereni, L., Shakil, S., St. Pierre, K., Thompson, L., and Zolkos, S.: A Consolidated Database
721 of Mercury Observations for Permafrost Regions, 2026. <https://zenodo.org/records/18301176>

722 Outridge, P. M., Mason, R. P., Wang, F., Guerrero, S., and Heimbürger-Boavida, L. E.: Updated
723 Global and Oceanic Mercury Budgets for the United Nations Global Mercury Assessment 2018,
724 *Environ. Sci. Technol.*, 52, 11466–11477, <https://doi.org/10.1021/acs.est.8b01246>, 2018.

- 725 Schaefer, K., Elshorbany, Y., Jafarov, E., Schuster, P. F., Striegl, R. G., Wickland, K. P., and
 726 Sunderland, E. M.: Potential impacts of mercury released from thawing permafrost, *Nature*
 727 *Communications*, 11, 4650, <https://doi.org/10.1038/s41467-020-18398-5>, 2020.
- 728 Schuster, P. F., Schaefer, K. M., Aiken, G. R., Antweiler, R. C., Dewild, J. F., Gryziec, J. D.,
 729 Gusmeroli, A., Hugelius, G., Jafarov, E., Krabbenhoft, D. P., Liu, L., Herman-Mercer, N., Mu,
 730 C., Roth, D. A., Schaefer, T., Striegl, R. G., Wickland, K. P., and Zhang, T.: Permafrost Stores a
 731 Globally Significant Amount of Mercury, *Geophysical Research Letters*, 45, 1463–1471,
 732 <https://doi.org/10.1002/2017GL075571>, 2018.
- 733 Sonke, J., Teisserenc, R., Heimbürger-Boavida, L., Petrova, M., Maruszczak, N., Le Dantec, T.,
 734 Chupakov, A., Li, C., Thackray, C., Sunderland, E., Tananaev, N., and Pokrovsky, O.: Eurasian
 735 river spring flood observations support net Arctic Ocean mercury export to the atmosphere and
 736 Atlantic Ocean, *PROCEEDINGS OF THE NATIONAL ACADEMY OF SCIENCES OF THE*
 737 *UNITED STATES OF AMERICA*, 115, E11586–E11594,
 738 <https://doi.org/10.1073/pnas.1811957115>, 2018.
- 739 Sonke, J., Angot, H., Zhang, Y., Poulain, A., Björn, E., and Schartup, A.: Global change effects
 740 on biogeochemical mercury cycling, *AMBIO*, <https://doi.org/10.1007/s13280-023-01855-y>,
 741 2023.
- 742 St. Pierre, K. A., Zolkos, S., Shakil, S., Tank, S. E., St. Louis, V. L., and Kokelj, S. V.:
 743 Unprecedented Increases in Total and Methyl Mercury Concentrations Downstream of
 744 Retrogressive Thaw Slumps in the Western Canadian Arctic, *Environ. Sci. Technol.*, 52, 14099–
 745 14109, <https://doi.org/10.1021/acs.est.8b05348>, 2018.
- 746 [Thompson, L. M., Shewan, R., Mangal, V., Harris, L. I., Cheng, C. H., Braga, L. P. P.,](#)
 747 [Kolmakova, O., Tanentzap, A. J., Knorr, K. H., Kuhn, M. A., Haugk, C., Azaroff, A., Jonsson,](#)
 748 [S., St. Louis, V. L., Lehnherr, I., Quinton, W. L., Sonnentag, O., & Olefeldt, D. \(2025\).](#)
 749 [Production of Methylmercury in Peatlands Following Permafrost Thaw Increases along a](#)
 750 [Trophic Gradient. *Environmental Science & Technology*, 59\(36\), 19457–19467. <https://doi->](#)
 751 [org.colorado.idm.oclc.org/10.1021/acs.est.5c04510](#)
- 752 [Tian, S., Li, D., Zhang, T., McClelland, J. W., Overeem, I., Lane, S. N., Spencer, R. G. M.,](#)
 753 [Wohl, E., Sha, A., Zhao, Y., Miao, C., Ning, M., Yuan, L., & Ni, J. \(2026\). Increasing river](#)
 754 [sediment concentration and flux across the pan-Arctic. *Nature Geoscience*, 1–8. <https://doi->](#)
 755 [org.colorado.idm.oclc.org/10.1038/s41561-026-01960-z](#)
- 756 Varty, S., Lehnherr, I., St. Pierre, K., Kirk, J., and Wisniewski, V.: Methylmercury Transport and
 757 Fate Shows Strong Seasonal and Spatial Variability along a High Arctic Freshwater Hydrologic
 758 Continuum, *Environ. Sci. Technol.*, 55, 331–340, <https://doi.org/10.1021/acs.est.0c05051>, 2021.
- 759 Virkkala, A., Natali, S., Rogers, B., Watts, J., Savage, K., Connon, S., Mauritz, M., Schuur, E.,
 760 Peter, D., Minions, C., Nojeim, J., Commane, R., Emmerton, C., Goeckede, M., Helbig, M.,
 761 Holl, D., Iwata, H., Kobayashi, H., Kolari, P., López-Blanco, E., Marushchak, M., Mastepanov,
 762 M., Merbold, L., Parmentier, F., Peichl, M., Sachs, T., Sonnentag, O., Ueyama, M., Voigt, C.,
 763 Aurela, M., Boike, J., Celis, G., Chae, N., Christensen, T., Bret-Harte, M., Dengel, S., Dolman,
 764 H., Edgar, C., Elberling, B., Euskirchen, E., Grelle, A., Hatakka, J., Humphreys, E., Järveoja, J.,

765 Kotani, A., Kutzbach, L., Laurila, T., Lohila, A., Mammarella, I., Matsuura, Y., Meyer, G.,
766 Nilsson, M., Oberbauer, S., Park, S., Petrov, R., Prokushkin, A., Schulze, C., St Louis, V.,
767 Tuittila, E., Tuovinen, J., Quinton, W., Varlagin, A., Zona, D., and Zyryanov, V.: The ABCflux
768 database: Arctic-boreal CO₂ flux observations and ancillary information aggregated to monthly
769 time steps across terrestrial ecosystems, *EARTH SYSTEM SCIENCE DATA*, 14, 179–208,
770 <https://doi.org/10.5194/essd-14-179-2022>, 2022.

771 Wohlgemuth, L., Rautio, P., Ahrends, B., Russ, A., Vesterdal, L., Waldner, P., Timmermann, V.,
772 Eickenscheidt, N., Fürst, A., Greve, M., Roskams, P., Thimonier, A., Nicolas, M., Kowalska, A.,
773 Ingerslev, M., Merilä, P., Benham, S., Iacoban, C., Hoch, G., Alewell, C., and Jiskra, M.:
774 Physiological and climate controls on foliar mercury uptake by European tree species,
775 *Biogeosciences*, 19, 1335–1353, <https://doi.org/10.5194/bg-19-1335-2022>, 2022.

776 Zhang, L., Qian, J.-L., and Planas, D.: Mercury concentration in tree rings of black spruce (*Picea*
777 *mariana* Mill. B.S.P.) in boreal Quebec, Canada, *Water Air Soil Pollut*, 81, 163–173,
778 <https://doi.org/10.1007/BF00477263>, 1995.

779 Zhang, Y., Zhang, P., Song, Z., Huang, S., Yuan, T., Wu, P., Shah, V., Liu, M., Chen, L., Wang,
780 X., Zhou, J., and Agnan, Y.: An updated global mercury budget from a coupled atmosphere-
781 land-ocean model: 40% more re-emissions buffer the effect of primary emission reductions, *One*
782 *Earth*, 6, 316–325, <https://doi.org/10.1016/j.oneear.2023.02.004>, 2023.

783 Zolkos, S., Krabbenhoft, D. P., Suslova, A., Tank, S. E., McClelland, J. W., Spencer, R. G. M.,
784 Shiklomanov, A., Zhulidov, A. V., Gurtovaya, T., Zimov, N., Zimov, S., Mutter, E. A., Kutny,
785 L., Amos, E., and Holmes, R. M.: Mercury Export from Arctic Great Rivers, *Environmental*
786 *Science & Technology*, 54, 4140–4148, <https://doi.org/10.1021/acs.est.9b07145>, 2020.

787